AIMS Materials Science, 10(3): 499–516.
DOI: 10.3934/matersci.2023028
Received: 05 April 2023
Revised: 25 May 2023
Accepted: 06 June 2023
Published: 26 June 2023

http://www.aimspress.com/journal/Materials

Research article

Understanding of low-carbon steel marine corrosion through simulation in artificial seawater

Yustina M Pusparizkita[1], Vivi A. Fardilah[2], Christian Aslan[3], J. Jamari[2] and Athanasius P Bayuseno[2,*]

[1] Department of Environmental Engineering, Faculty of Engineering, Diponegoro University, Semarang, Indonesia
[2] Department of Mechanical Engineering, Faculty of Engineering, Diponegoro University, Semarang, Indonesia
[3] Department of Chemical Engineering, Faculty of Industrial Technology, Institut Teknologi Bandung, Bandung, Indonesia

* **Correspondence:** Email: apbayuseno@gmail.com; Tel: +62-024-7460059; Fax: +62-024-7460059.

Abstract: The current laboratory experiments investigated the corrosion resistance of carbon steel in artificial seawater (ASW) using the steel coupons hanging on a closed glass reactor of ASW with volume-to-specimen area ratios ranging from 0.20 to 0.40 mL/mm^2. These coupons were immersed in ASW for varying time durations (7 and 14 d) at room temperature without agitation. Further, the corrosion rates based on the weight loss and electrochemical analytical method were determined. Following exposure to carbon steel for 7 and 14 d, corrosion rates were 0.2780 *mmpy* and 0.3092 *mmpy*, respectively. The surfaces appeared to be not protected by oxides based on this result. The electrochemical impedance spectrometer in potentiostatic/galvanostatic mode, in conjunction with EDX analysis, predicted the evolution of oxygen reduction. The 7th-day immersion sample had a higher oxygen content, and the 14th-day immersion sample had a slightly lower oxygen content. Methods of X-ray diffraction (XRD) and scanning electron microscopy (SEM) characterized the surface morphology and composition of their corrosion product. Corrosion products derived from rust minerals hematite, lepidocrocite and magnetite appeared to cover the carbon steel surface after exposure. This result can get insight into the corrosion behavior of low-carbon steel used in marine environments.

Keywords: corrosion; low carbon steel; artificial seawater; a closed reactor; rust minerals

1. Introduction

Carbon steels are a common material used in construction, with carbon levels varying in each steel. Steel carbon levels follow three categories: low-, medium and high carbon content. Low-carbon steel typically contains a carbon content of 0.25%–0.30% [1]. The low-carbon steels are the most common materials used in marine engineering equipment because of their excellent mechanical strength, ease of manufacture, weldability and formability [2,3]. These steels are highly formable because they contain very little carbon, typically less than 0.30% C and up to 0.4% Mn [1,4]. Compared to other types of steel, low-carbon steel is the preferred construction material used today; it is commonly used in marine engineering [5]. Nonetheless, the carbon steel used in engineering facilities exposed to the marine environment is vulnerable to serious corrosion risks [5–8].

In general, corroded carbon steel causes degradation of the material properties when exposed to a corrosive environment, resulting in weight loss and reduced material strength [9,10], which is a potentially catastrophic problem, particularly for marine engineering structures. Further, many engineering types of equipment made from carbon steel, such as oil and gas platforms, seawater desalination systems, submarine cables, bridges and submarine transportation pipelines, are susceptible to corrosion [11,12]. Metal corrosion in marine systems can be general or localized, resulting in a high corrosion cost in terms of preventive inhibitors. Furthermore, corrosion in seawater can cause significant economic losses due to lost production, product loss, efficiency loss and contamination. According to NACE International research, corrosion cost can contribute between 3.5% and 5.2% of global GDP (4.35% on average). Corrosion costs about 1–4% of a developed country's GDP [13]. Furthermore, the cost of seawater corrosion may correspond to toxic substance leakage, which influences the environment and human health. As a result, corrosion-related deterioration of coastal steel infrastructure has become a focus of research into corrosion-resistant materials and enhanced corrosion mitigation strategies [14].

Seawater is typically aggressive corrosive media for corrosion, whereas this corrosion mechanism depends on chemical, biological and physical factors. The salt content in seawater is higher than in freshwater, which directly controls water conductivity and oxygen content. Ocean water has a salinity of 3.5% on average [15]. The concentration of [Cl^-] ions in water is mainly related to salinity. Here, chloride in seawater can destroy oxide layers on metal surfaces, forming complex metal ions, producing hydrogen ions during hydrolysis, increasing seawater acidity and strengthening local metal corrosion. However, nearly ionized salt has a high electrolyte conductivity which can accelerate microcrystalline and macrocrystalline corrosion mechanisms.

Additionally, the form of corrosion in seawater is related to oxygen and carbon dioxide concentrations. Carbon dioxide changes the pH of seawater, making it more acidic. In this case, oxygen acts as a depolarizer in the cathodic half-cell, increasing the risk of corrosion. The greater the concentration of dissolved oxygen in the sea, the greater the electron capacity of the metal produced and the faster the metal corrodes. Oceanic water has a pH ranging from 7.3 to 8.6 [16]. The corrosion behavior of passive metals will be affected by the pH range observed in seawater [17]. At pH levels ranging from 1 to 8, the oxygen system typically controls the oxidation and reduction potential of the

seawater.

Further, extensive research on carbon steel corrosion behavior in seawater has recently been conducted and evaluated on the effect of induced stress. Correspondingly, the impact of induced stresses on steel corrosion behavior in marine environments has been reported previously [18–20]. Specifically, corrosion studies on low-carbon steels A131/A and A131/AH32 in simulated seawater environments have previously been reported [3,4]. A field study on the corrosion behavior of AISI 4135 steel in exposure to marine environments has also been reported [21]. Moreover, the corrosion evolution and stress corrosion cracking (SCC) behavior of E690 steel in the electrolyte presence of the simulated marine environment was also intensively researched [22]. Following that, the use of a coastal-industrial atmosphere for corrosion media of investigation in corrosion kinetics and product layer evolution of galvanized steel submitted to a wet/dry cyclic corrosion test was reported by Qiao et al. [23]. Depth understanding of the corroded surface carbon steel in natural seawater and the relationship between the composition of these layers and the corrosion mechanisms were studied by Refait et al. [24]. Recent advances in the depth understanding of localized corrosion processes of carbon steel permanently immersed in natural seawater have been established through a detailed analysis of the corrosion product layers [25–30]. Yan et al. [31] have successfully predicted the corrosion rate and influencing factors evaluation of low-alloy steels in the marine atmosphere using a machine-learning approach. Because hydrogen ions play a significant role in seawater corrosion processes, an intensive study had performed on the rate of hydrogen absorption and hydrogen diffusion in ferritic steel coated with ZnNi [32]. At the same time, other study had conducted on the effects of microstructures and grain size of mild steel on the corrosion resistance of carbon steel [33]. As carbon steel is found widely in marine constructions, many types of carbon steel were corrosion tested under varying marine environments. Accordingly, understanding the unique properties of different carbon steel is crucial for managing the corroding process in the marine environment. This scientific knowledge is required to meet the technological goals of accurately anticipating corrosive substance loss in this environment and determining the life expectancy of low-carbon steel structures.

Despite varying results for corrosive environments in different sea areas and duplicating all *in situ* seawater variables, in situ marine corrosion experiments are still the most reliable method for studying corrosion in seawater environments. As a result, a laboratory experiment is a viable method for seawater corrosion of metals and alloys, which has the advantages of a short testing period, low experimental cost, easy operation and high reproducibility because the corrosive environments of different sea areas are vastly different [25,34–39] Furthermore, it was proposed in terms of present research that the carbon steel corrosion was hypothetically related to the oxygen content in seawater and was almost unaffected by pressure. The difference in crevice corrosion between the two site metallic samples might be due to a difference in oxygen content previously reported using seawater from the Pacific (1.6 mL/L) and the Atlantic (5.7 mL/L) ocean [40].

Accordingly, this study included a short-term in-situ marine corrosion experiment with corrosion-resistant low-carbon steel in seawater. The current study used a simple and quantitative analytical method to evaluate the corrosion behavior of AISI 1010 in simulated seawater. The novelty and rationale of the present work were related to the link between investigating the effect of oxygen content in artificial seawater and the corrosion results of carbon steel. This study used electrochemical measurement, gravimetric, scanning electron microscopy (SEM) and X-ray diffraction (XRD) to characterize corroded low-carbon steel AISI 1010 surfaces. This study can add

valuable data and guidance for material selection for oil and gas pipelines in coastal areas.

2. Materials and methods

2.1 Material, Medium and In-situ marine experiment

Specimens employed for this experiment were AISI 1010 low-carbon plates of steel having the elemental chemical composition listed in Table 1. Sample coupons cut into 1.5 cm × 1.5 cm × 0.5 cm in size were for weight loss analyses. Other coupons of the same size were placed in epoxy resin inside a PVC pipe for electrochemical measurements, with a working surface area of 2.25 cm^2 (Figure 1a). Polishing surface coupons were conducted with silicon carbide metallurgical papers with grid sizes ranging from 240 to 1200, degreased with ethanol and dried by electric dryers. A desiccator was employed to test the polished coupons for corrosion.

Table 1. Chemical composition of AISI 1010 carbon steel (wt%).

Grade	C	Mn	Ti	Al	Si	Cr	Ni	Cu	Co	Fe
AISI 1010	0.04	0.33	0.003	0.013	0.02	0.013	0.017	0.0082	<0.005	Balance

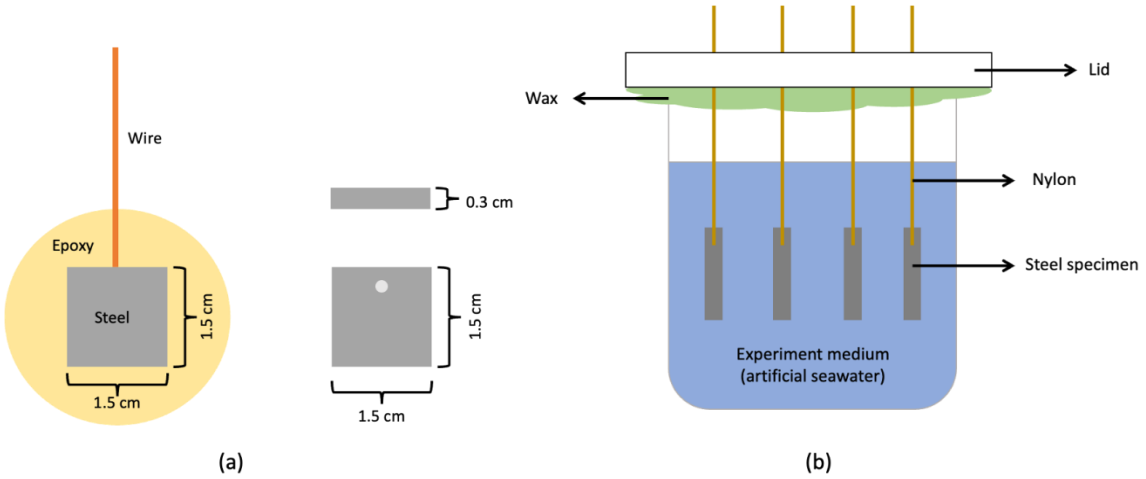

Figure 1. (a) The shape of the steel specimens; (b) Schematic set up for immersion process.

The artificial seawater (ASW) in this study is according to ASTM D1141, and its chemical composition (g/L) is shown in Table 2. Adding 5% sodium hydroxide resulted in a pH solution of 8.2. Figure 1b depicts the schematic diagrams of the in-situ marine experiment in this study. The experimental reactor had two components: the reactor and the lid. The glass reactors have a total volume of 400 mL and are sealed with an acrylic top, while specimens are suspended by hanging with nylon string. The “solution volume to specimen area" ratio was 0.20–0.40 mL/mm^2 according to ASTM G 31-72, so the maximum coupons with dimensions of 1.5 cm × 1.5 cm × 0.3 cm were four specimens for a working volume of 350 mL. Subsequently, the reactor was closed with wax during immersion and lasted 14 d at room temperature.

Table 2. Chemical composition of ASW (g/L) according to ASTM D1141.

NaCl	$MgCl_2$	Na_2SO_4	$CaCl_2$	KCl	$NaHCO_3$	KBr	H_3BO_3	$SrCl_2$	NaF
24.53	5.2	4.09	1.16	0.695	0.201	0.101	0.027	0.025	0.003

2.2. Electrochemical and weight loss measurement

The computer program run with the CS Studio 5 software performed all electrochemical measurements with the Potentiostat/Galvanostat (CorrTest Type CS 300). The OCP and Tafel analysis tests determined the corrosion rate of the carbon steel samples. The electrochemical measurements used three-electrode cells, including platinum (Pt) as the reference electrode and silver-silver chloride (SSCE)/(Ag/AgCl) as counter electrodes. The un-corroded or corroded steel specimens with an exposed area of 2.25 cm^2 are working electrodes. Polarization data collection focused on the range voltage of 0.2 V to +0.2 V vs. open circuit potential range at a constant scan rate of 10 mV/ min. Generating a linear fitting method may obtain the electrochemical parameters of ba, bc, Icorr and Ecorr (Tafel slope of the anodic reaction and the cathodic reaction, corrosion current density and corrosion potential) of each sample at the weak polarization region (±20 mV vs. Ecorr).

Further, the weight loss (gravimetric) method was for determining corrosion rates of AISI 1010 steel simulated in the ASW and two samples of similar dimensions standard as parallel samples for each experiment set. After ending the immersion test in the simulated seawater on the 7th and 14th day, steel was washed with distilled water, gently scraping off corrosion products and eventually descaling with a pickling solution. According to ASTM G1-90, cleaning corrosion products employed a pickling solution (Clarke solution) (20 g Sb_2O_3 and 50 g $SnCl_2$ in 1 L of 6 N HCL). After descaling, the steel was washed with distilled water and ethanol, then dried with an electric dryer. The difference in metal weight measured before and after immersion and pickling determined corrosion rates.

2.3. Corroded surface steel characterizations

The morphology of the corrosion products was studied using scanning electron microscopy (SEM, Hitachi SU3500). The study includes SEM images of steel surfaces after 14 d of immersion. The samples were dehydrated using aqua-dm and serial ethanol dilutions (20%, 50%, 75% and 98%). All coupon specimens were then dried and placed in desiccators. Before SEM observation, a thin gold film of 0.5 mm thickness was deposited on the specimen surface to give electrical conductivity, and SEM images were at various magnifications to take.

Instead, XRD analysis was to evaluate the crystalline corrosion products on the surface of the steel sample after immersion. (XRD-Bruker D8 method). The corroded metals were therefore dried and stored in a desiccator before being exposed to X-ray beams emitting Cu-Kα (λ = 0.154 nm) radiation with a 2θ scan between 10 ° and 90 °. The QualX PC-search-match tool [41] software package aids in crystalline material identification. Using the crystal structure model in the literature, the Rietveld refinement approach with Program X'Pert plus 1.0 (Philips Analytical B.V.) confirmed the discovered crystalline phases of the search match method. (AMCSD-American Mineralogist of crystal structure database) [42].

3. Results

3.1. Corrosion rates

Table 3 shows the steel corrosion rates of specimens after an immersion test time of the 7th and 14th day in ASW-based weight loss analyses. Overall, corrosion rates appeared to increase according to the length of the immersion time. There were no corrosion inhibitors used in the study area. In this study, electrochemical analyses of corrosion rates provided results faster than rates of the weight loss methods (Figure 2), presenting the polarization curve of the specimen measured in the ASW at various immersion times. The longer the immersion time, the greater the negative value of Ecorr became, eventually reaching −0.613 V on day 14. These findings suggested that the marine environment of ASW promoted an increase in corrosion rates for low-carbon steel during immersion. Table 4 shows the corresponding polarization curve adjustment results for this work. Icorr values appeared to increase until they reached 24.733 A/cm^2. The highest Icorr values, however, were obtained after the 7th day rather than the 14th day of immersion (19.841 A/cm^2). These findings were in close agreement with the result of the corrosion rates calculation based on the weight loss procedure. After the 7th day of immersion, the metal corrosion rate increased significantly, from 0.0954 *mmpy* to 0.2879 *mmpy*. Then, the corrosion rate dropped slightly on the 14th day to 0.231 *mmpy*.

Table 3. Corrosion rate of AISI 1010 based on weight loss.

Immersion time (day)	Average weight loss (%)	Corrosion rate (*mmpy*)
7	0.07%	0.2780
14	0.16%	0.3092

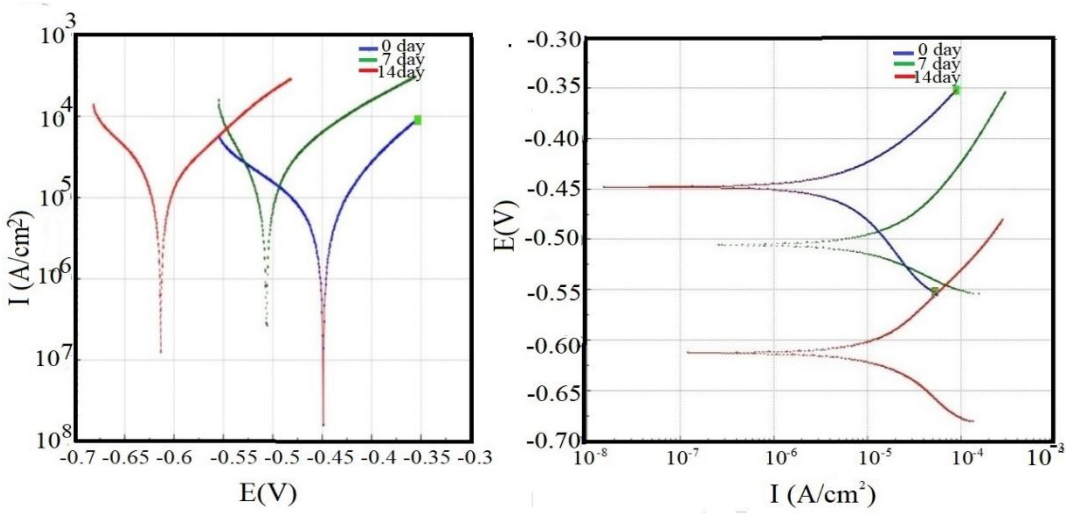

Figure 2. The polarization curve of AISI 1010 in the ASW.

Table 4. Polarization measurement of AISI 1010 in ASW.

No.	Material (Low carbon steel)	Immersion time (day)	Corrossion rate (*mmpy*)	I_{corr} ($\mu A/cm^2$)	E_{corr} (V)	βa (mV)	βc (mV)	Residual
1	AISI 1010	0	0.0954	8.198	−0.506	88.126	147.56	1.58E-9
2	AISI 1010	7	0.2879	24.733	−0.449	134.81	82.096	2.69E-8
3	AISI 1010	14	0.2310	19.841	−0.613	113.8	88.839	7.16E-9

In this study, according to the results of the electrochemical analysis, the first seven days of corrosion rate increased rapidly compared to the next seven days of the mass loss method (the increase in corrosion rate here was only 0.0312 *mmpy* and reached 0.3092 *mmpy*). Instead, the corrosion rate of the specimen based on the electrochemical analysis increased significantly in the first seven days but decreased in the following seven days. Several materials corrode rapidly in the early stages of exposure to an environment (before passive film formed) and later corrode at a much lower rate [43].

In gravimetric or weight loss measurement, there was involving step, namely, the removal of corrosion products (pickling). This step is essential to accurately measure the weight loss due to corrosion, as it eliminates the interference of passive films or corrosion products. More corrosion products formed on the metal surface on day 14th than those on day 7th can provide by the value of mass loss during the pickling process (Table 3). As a result, the weight of the specimen remained decreased. A higher loss of metal mass indicates an increased corrosion rate. The increase in corrosion rate in the first seven days corresponded to a lack of protective coatings on the metal surface and the corrosive nature of the medium. The most well-known situation is metal corrosion (electrochemical) in aquatic environments (water-containing environments), including dissolved species (salts) [44]. However, gravimetric analysis does not provide detailed information about the corrosion mechanism. The gravimetric method does not allow the evaluation of quantitative estimation of the corrosion rate for each layer separately [45]. As a more detailed understanding of corrosion mechanisms is required, complementary techniques such as electrochemical methods may be necessary.

Electrochemical corrosion testing is a relatively rapid technique to estimate the corrosion response of a material when exposed to a particular environment. The electrochemical method is particularly to reveal the rate of the step-controlling process, calculate the mass corrosion index and substantiate the choice of a protector for a specific aggressive medium. In the experiment, the polarization curves refer to the mass corrosion indices of the layer components [46,47]. An exergonic process because metals tend to have the lowest energy levels. As a result, when metals like steel combine with oxygen and water, they naturally return to their lowest energy state and form iron oxides (corrosion products). However, corrosion products may have different properties depending on the specific metal and the conditions. The formed corrosion products revealed the surface of the corroded metal over time. Then, metal surfaces can form dense and adhering layers that create physical barriers between metals and corrosion environments. The barrier layer formed from an accumulation of corrosion products can prevent metals from directly touching the corrosive agent and slowing metal corrosion. Dense corrosion product layers act as a weight transport barrier, reducing corrosion rates significantly [48]. According to the results of Chen et al. [49] for electrochemical measurement, the accumulation of corrosion products may play a significant role in protecting carbon steel in sterile seawater. Accordingly, inhibiting corrosion of carbon steel is due to accumulating corrosion product film in a sterilized environment. More corrosion products building thick and complete layer has adhered to the surface of carbon steel, limiting charge transfer in sterile seawater [49,50]. In this

situation, the barrier layer delays the electrochemical reactions that cause corrosion and provides some metal protection, resulting in a lower corrosion rate as measured by polarization (Table 4). Surface morphology SEM data show the presence of this layer.

3.2. Surface morphology and chemical elemental mapping

SEM images of corrosion product distribution showed existing corrosion products on AISI 1010 surfaces (Figure 3). Within a relatively short period of immersion, corrosion product spots appeared on corroded surface samples; on the seventh day, the surface rust thickened and became unevenly distributed. Despite uneven thicknesses, corrosion products obtained on the 14th day almost covered the entire surface. Moreover, the EDX spectra reflect the distribution of rust minerals (Figure 4). Here the forming corrosion products of metals in seawater and marine environments are primarily iron oxides [51–57]. The percentages of iron and oxygen contents related to the weight of rusting material are on different color images of the chemical elements available in the samples. EDX spectra revealed 67 wt% of Fe and 19 wt% of oxide concentrations on the uncorroded coupons before immersion. However, the oxide concentrations increased to 47 wt% on the 7th day, while the Fe concentration decreased to 44 wt% on the 14th immersion, as the amount of corrosion (rust) products increased and the corrosion rate decreased. This finding is consistent with the corrosion rate investigation. The slight decrease in the 14th-day corrosion rate previously observed by the weight loss method matched the EDX analysis with a drop of 39 wt% in oxide concentration.

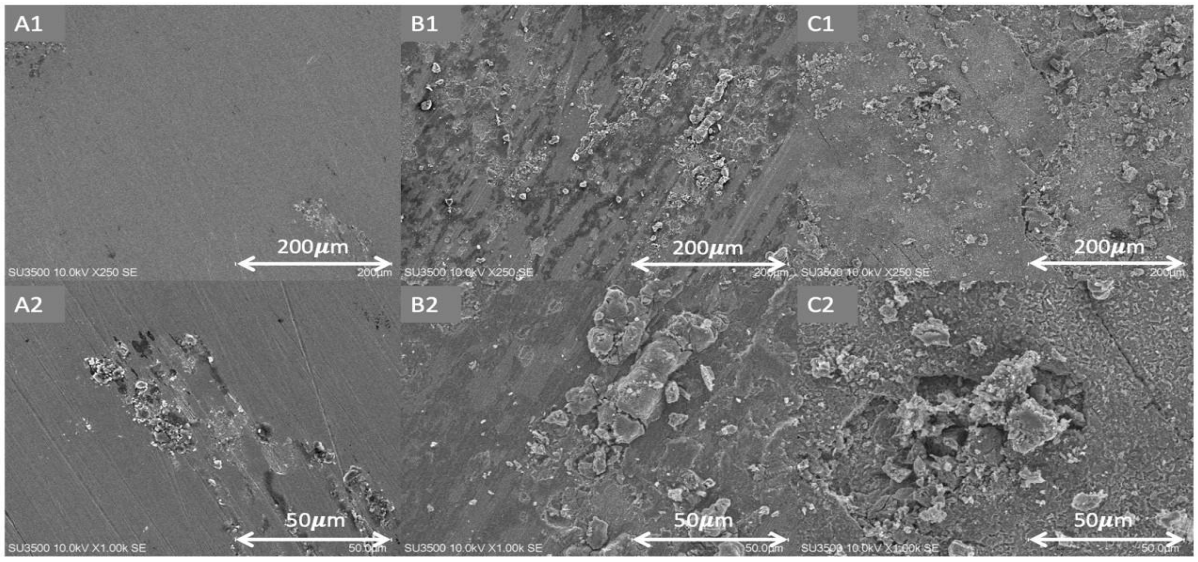

Figure 3. SEM images of AISI 1010 corrosion in ASW at 250 and 1000× magnification (A1&2) after 0 d, (B1&2) after 7 d and (C1&2) after 14 d.

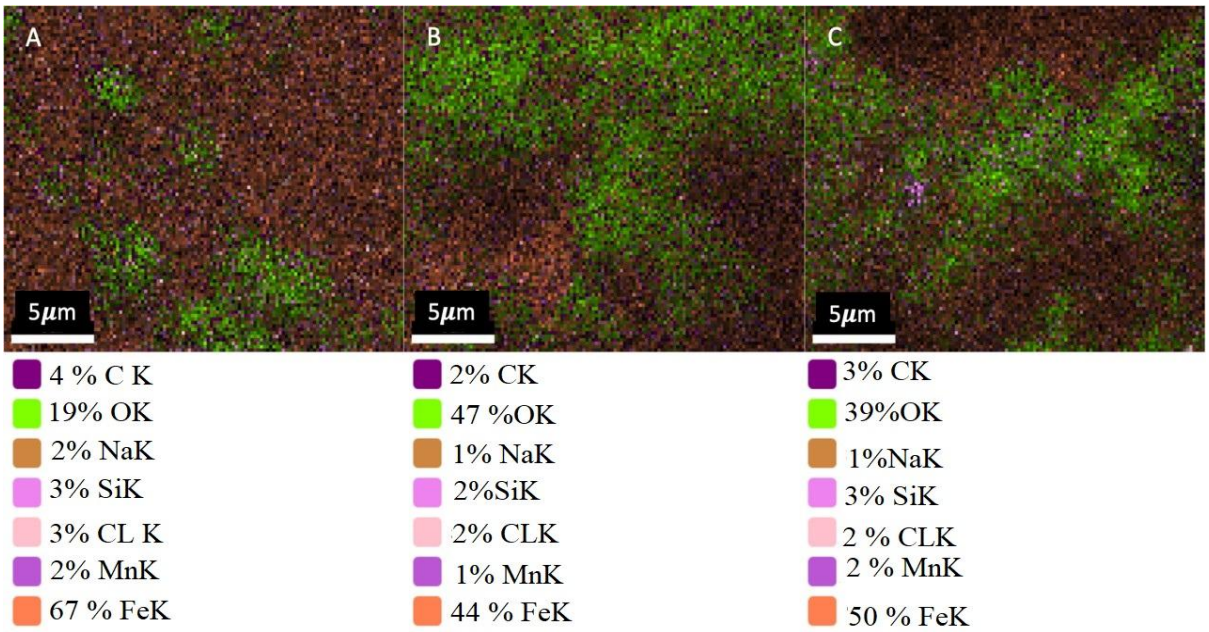

Figure 4. SEM/EDX images of AISI 1010 corrosion in ASW (A) 0 days (B) 7 d and (C) 14 d.

3.3. Corrosion products of AISI 1010 in seawater

The shape of corrosion product particles can predict the type of corrosion product formed. It appears that rust on the steel coupon surface has two distinct layers: a dense layer immediately adjacent to the base Fe-metal and a relatively thin layer (Figure 3). After immersion in ASW, the shape of the corrosion product shows an enlargement of hematite (Fe_2O_3), magnetite (Fe_3O_4) and lepidocrocite [γ-FeO(OH)], suggested to be corrosion products (Figure 5). Corrosion products frequently exist by rust minerals such as Fe_3O_4 and Fe_2O_3 [50]. EDX spectra confirmed the Fe and O spectra corresponding to compounds of iron oxides (II) and iron oxides (III), which formed easier on the surface due to their high oxygen affinity.

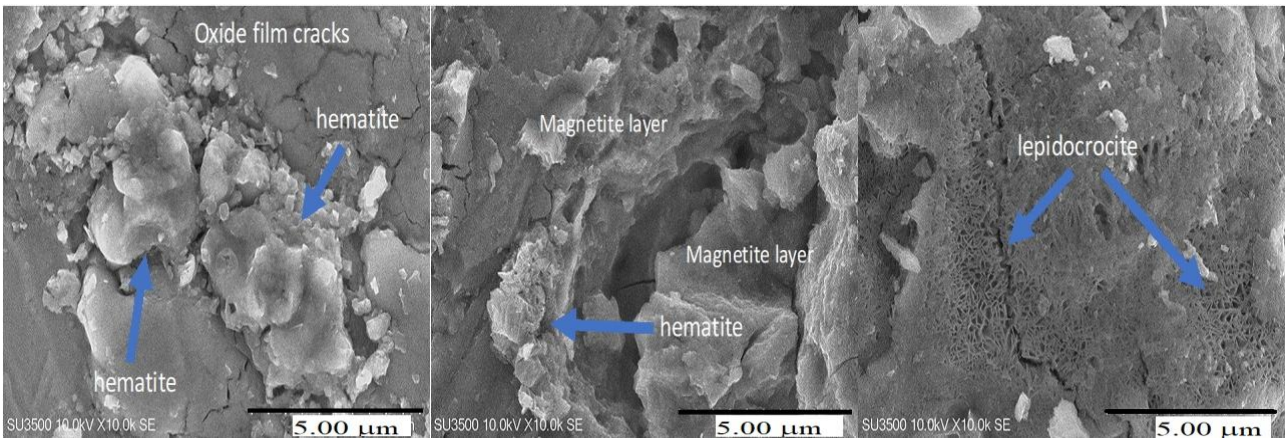

Figure 5. The visual appearance of AISI 1010 corrosion products in ASW.

Further, hematite is a mineral substance with a reddish-brown appearance consisting of ferric oxide. Hematite is one of the corrosion products that can form on the surface of iron or steel materials and is the most stable phase when exposed to oxidizing environments [55]. The appearance of hematite in Figure 5 agreed with the image obtained by the previous finding of Mohammadikish [58]. On the other hand, magnetite is also identified from observations of oxidation-inducing corrosive product forms and becomes hematite (Eqs 1 and 2). According to the previous result by Antunes et al. [59], the magnetite pattern comes out as dark flat regions. Magnetite can be compact and protective in the absence of oxygen. In addition, magnetite is usually favorable to form as a second component in low-oxygen components near the metal matrix, controlling the entire corrosion process [59]. As an iron oxide-hydroxide mineral, lepidocrocite is green hematite or emeraldine and is formed as iron-containing substances rust underwater. Here lepidocrocite crystal structure is like the boehmite structure found in bauxite and consists of layered iron (III) oxide octahedral bonded by hydrogen bonding via hydroxide layers. Lepidocrocite is the corrosion product of carbon steel in sterilized artificial seawater [60]. The relative content of lepidocrocite increases with immersion time in sterile seawater [49]. Previous studies indicated that the formation of global and thin laminas corrosion products corresponded to lepidocrocite formation, which agrees with our observation in Figure 5 [55,60]. In addition to iron hydroxides, SEM images revealed clear and distinct oxide films on the surface (Figure 5), which eventually branched into cracks encountered due to the breaking of the thin films during corrosion. Based on the result of Liu et al. [61], the characteristics of the surface film can act as a barrier consisting of rust solid products with visible slight cracks.

Even though seawater corrosion of the surface metal can take many forms, seawater is an electrolyte for metal electrochemical corrosion, resulting in oxygen reduction in the surface metal (Figure 6). It was proposed in the study that during marine corrosion in seawater, the steel surface forms oxides and hydroxides of iron according to the reduction-oxidation reactions (Eqs 3 and 4) [62].

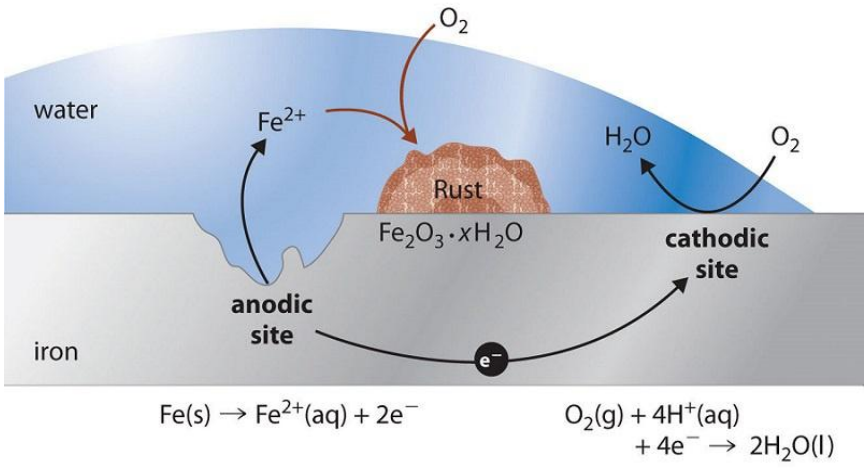

Figure 6. The electrochemical cell set up between anodic and cathodic sites on an iron surface corrodes (CC BY-NC-SA; anonymous).

$$4Fe + 3O_2 + 2H_2O_4 \rightarrow FeOOH \quad (1)$$

$$2FeOOH \rightarrow Fe_2O_3 + H_2O \quad (2)$$

$$Fe + \frac{1}{2}O_2 + H_2O \rightarrow Fe(OH)_2 \quad (3)$$

$$Fe(OH)_2 + \frac{1}{2}O_2 \rightarrow Fe_3O_4 + 3H_2O \quad (4)$$

Moreover, the present results of rust minerals were in close agreement with identified different types of oxides that may form on the steel surface: hematite (α-Fe_2O_3), magnetite (Fe_3O_4), maghemite (γ-Fe_2O_3), goethite (α-FeOOH), lepidocrocite (γ-FeOOH), akaganeite (β-FeOOH), feroxyhite (δ-FeOOH), iron hydroxide [$Fe(OH)_2$] and iron trihydroxide ($Fe(OH)_3$) [62–64]. The formation of lepidocrocite occurs by the re-oxidation of magnetite, which is the reaction according to Eq 5 [65]. Lepidocrocite usually transforms to its more stable polymorphic goethite governed by the topotactic process in Fe^{2+} systems [66]. A detailed review of the marine corrosion of carbon steel by Alcántara et al. [65] mentioned lepidocrocite formation as a primary corrosion product in the atmospheric rust layer.

$$Fe_3O_4 + \frac{3}{2}O_2 + H_2O \rightarrow 3\gamma - Fe00H \quad (5)$$

The XRD Rietveld analysis in Figure 7 supports the SEM-based corrosion products by demonstrating the low intensity of the diffraction peaks produced by the rust's thin thickness. Hematite and magnetite can form in oxidizing environments, whereas lepidocrocite can form in reducing environments. As a result, hematite, lepidocrocite and magnetite may be corrosion products formed during ASW immersion.

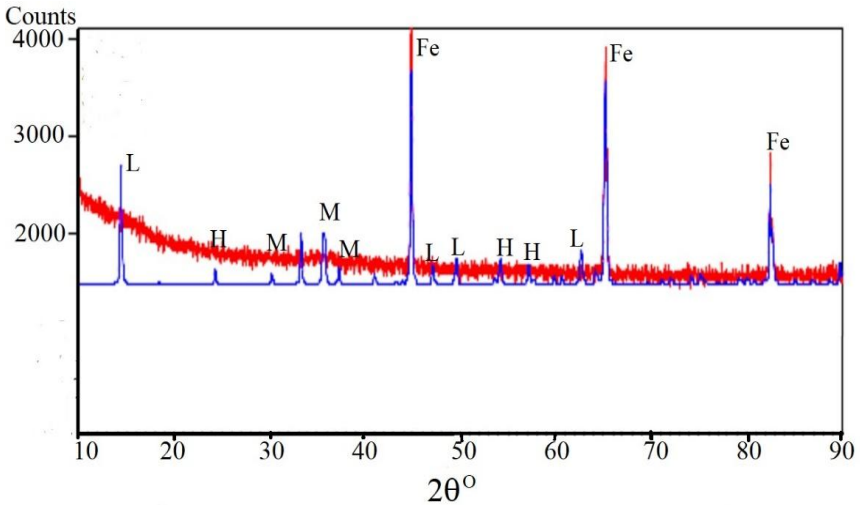

Figure 7. XRD Rietveld analysis of corroded carbon steel (based on Fe) after a 14-day immersion revealed rusting minerals H (hematite), L (lepidocrocite) and M. (magnetite). Notes: The blue line spectra represent the crystal structure model, and the red line spectra represent the measured XRD spectra.

4. Discussion

Electrochemical corrosion of low-carbon steel surfaces in seawater is of particular interest to avoid a catastrophic structure when used in marine applications. Understanding the mechanism of seawater corrosion and the development of corrosion inhibitors, in particular, have received much attention, as have the reduction-oxidation reactions that occur at the interfaces between the corrosive electrolyte and a steel surface during the early stages of the corrosion process. The nature and properties of the carbon steel surface, in particular, have been strongly affected by these reactions. As a result, recent corrosion and corrosion-inhibition studies on corrosion-resistant metal alloys in seawater environments have been conducted [38,67]. Furthermore, most corrosion studies refer to *in-situ* corrosion experiments with electrochemistry characterization of materials and surface properties.

Furthermore, the roles of chemical (oxygen content, salinity and pH), physical (temperature and agitation speed) and biological factors for seawater corrosion must take into account when considering the carbon steel surface, where seawater attacks the metallic surfaces controlling the amount of corrosion product presented as weight loss, corrosion rate and external corrosion of carbon steel [65]. Here a carbon steel pipe used in seawater may promote water-electrolyte formation by a current flow on its outer surface due to high and low potential, resulting in a microcell formation. The electrochemical impedance spectrometer with potentiostatic/galvanostatic mode could predict the evolution of oxygen reduction in this study, combined with an EDX analysis demonstrating that catalase aids processes for autocatalytic oxygen reduction and oxygen consumption. The higher the oxygen content in interfaces promoted faster the corrosion rate corresponding to the local anode corrosion rate depending on the cathodic reaction increases as the higher amount of oxygen. With an oxygen content of 4.85 mg/L in artificial seawater, the cathodic corrosion is predominantly by oxygen reduction, which is under mixed activation-diffusion control [68]. The initial increase in the oxygen reduction current on the 7th day of immersion is related to oxygen generation within the electrolyte, which can be produced by disproportioning hydrogen peroxide to water and oxygen. The current study demonstrated that the different concentrations of oxygen obtained from the varying day (7 and 14) of immersion provided varying weight losses, corrosion rates and external surface corrosion of metal specimens presented as rust minerals (hematite, lepidocrocite and magnetite).

Additionally, salinity (the amount of salt in seawater) regulates external metal corrosion. Because diluted seawater has low salinity, the electrolyte is not aggressive. However, because the current experiments only used one type of ASW, the influence of the salinity of seawater on carbon steel corrosion was insignificant. It is also important to note that common saturated carbonate accelerates seawater corrosion of carbon steel piping by increasing the pH level of seawater in contact with the protective carbonate mud. In this case, the pH of seawater decreases as the hydrostatic pressure in the seawater rises. As a result, a subsea pipeline may be unprotected by carbonate mud, which may not accelerate the corrosion rates. Photosynthesis has an impact on pH as well. For example, in subsea pipeline risers, proximity to water increases photosynthesis intensity and affects pH value, accelerating riser corrosion.

However, the current study focused solely on surface analytical techniques for characterizing corroded carbon steels in ASW media. This study has not yet evaluated factors such as dissolved oxygen content, bacterial species and temperature, which are significantly different from those found

in the marine environment below 500 m, and how they affect the corrosion behaviors of corrosion-resistant carbon steel. One of the significant areas for oil and gas development is the offshore area under seawater for a depth of approximately 170 m. As a result, more research needs on emerging surface analysis techniques and their applicability to investigating the corrosion behavior of carbon steels under the influence of seawater depth based on dissolved oxygen content, bacterial species and temperature. Additional work could involve advanced surface analytical techniques to measure temperature and oxygen content in seawater at depths in offshore areas, then replicating these conditions in situ in carbon steel corrosion experiments. Extending marine corrosion studies on carbon steel surfaces considering many corrosion factors (biological, chemical and physical) using existing and emerging surface analytical methods can help to fill gaps in our understanding of marine corrosion and corrosion inhibition mechanisms. Such knowledge is essential for developing reasonable material selection and design corrosion inhibition to ensure the safe operation of submarine oil and gas pipeline facilities throughout their life cycles and the corrosion behavior of pipelines in seawater retention environments.

5. Conclusions

A laboratory corrosion experiment of AISI 1010 low-carbon steel simulated in ASW revealed that the oxygen content influences the severity of localized metal substrate damage. According to electrochemical impedance spectrometer measurements, the corrosion damage caused by oxygen reducing to iron dissolution is due to oxidizing in the metal interface of the consumption of O_2 to H_2O. An oxygen uptake mechanism for oxygen reduction via iron dissolution may reduce biofilm adhesion to the metal substrate. However, the current study did not thoroughly investigate the biological, chemical and physical factors related to seawater depth. Therefore, further work should be conducted by considering many corrosion variables and advancing surface analytical methods for marine corrosion studies of carbon steel surfaces by duplicating those variables in *in-situ* corrosion experiments.

Use of AI tools declaration

The authors declare they have not used Artificial Intelligence (AI) tools in the creation of this article.

Acknowledgments

The authors would like to express their gratitude to Diponegoro University for providing financial support through the International Research Publications (RPI) program in the years 2022-2024 under grant contract No. 753-31/UN7.D2/PP/IX/2022. Also, thanks to the Electron Microscope Laboratory at the ITB's Research Centre for Nanoscience and Nanotechnology for assisting with data collection from the electron microscope.

Conflict of interest

The authors declare no conflict of interest.

References

1. Islam T, Rashed HMMA (2019) Classification and application of plain carbon steels, *Reference Module in Materials Science and Materials Engineering*, Elsevier. https://doi.org/10.1016/B978-0-12-803581-8.10268-1
2. Hamzah E, Hussain MF, Ibrahim Z, et al. (2014) The corrosion behavior of carbon steel in a seawater medium in presence of *P. aeruginosa* bacteria. *Arab J Sci Eng* 39: 6863–6870. https://doi.org/10.1007/s13369-014-1264-7
3. Mostafanejad A, Iranmanesh M, Zarebidaki A (2019) An experimental study on stress corrosion behavior of A131/A and A131/AH32 low carbon steels in simulated seawater. *Ocean Eng* 188: 106204. https://doi.org/10.1016/j.oceaneng.2019.106204
4. Singh R (2020) 6-Classification of steels, *Applied Welding Engineering*, 3rd Eds., Butterworth-Heinemann, 53–60. https://doi.org/10.1016/B978-0-12-821348-3.00014-8
5. Huang H, Jia C, Zhao O, et al. (2023) Local corrosion morphology analysis and simplification of low carbon steel plates. *Ocean Eng* 268: 113372. https://doi.org/10.1016/j.oceaneng.2022.113372
6. Bhandari J, Khan F, Abbassi R, et al. (2015) Modelling of pitting corrosion in marine and offshore steel structures—A technical review. *J Loss Prev Process Ind* 37: 39–62. https://doi.org/10.1016/j.jlp.2015.06.008
7. Dong B, Liu W, Zhang T, et al. (2021) Corrosion failure analysis of low alloy steel and carbon steel rebar in the tropical marine atmospheric environment: Outdoor exposure and indoor test. *Eng Fail Anal* 129: 105720. https://doi.org/ 10.1016/j.engfailanal.2021.105720
8. Zheng S, Zhang X, Zhao X (2019) Experimental investigation on seismic performance of corroded steel columns in the offshore atmospheric environment. *Struct Des Tall Spec Build* 28: e1580. https://doi.org/10.1002/tal.1580
9. Sherif ESM (2013) Comparative study on the inhibition of iron corrosion in aerated stagnant 3.5 wt% sodium chloride solutions by 5-Phenyl-1H-tetrazole and 3-Amino-1,2,4-triazole. *Ind Eng Chem Res* 52: 14507–14513. https://doi.org/10.1021/ie400725z
10. Song Y, Jiang G, Chen Y, et al. (2017) Effects of chloride ions on corrosion of ductile iron and carbon steel in soil environments. *Sci Rep* 7: 6865. https://doi.org/10.1038/s41598-017-07245-1
11. Ahn J-H, Choi WR, Jeon SH, et al. (2016) Residual compressive strength of inclined steel tubular members with local corrosion. *Appl Ocean Res* 59: 498–509. https://doi.org/10.1016/j.apor.2016.07.002
12. Feng L, He J, Hu L, et al. (2020) A parametric study on effects of pitting corrosion on steel plate's ultimate strength. *Appl Ocean Res* 95: 102026. https://doi.org/10.1016/j.apor.2019.102026
13. Lv M, Du M, Li X, et al. (2019) Mechanism of microbiologically influenced corrosion of X65 steel in seawater containing sulfate-reducing bacteria and iron-oxidizing bacteria. *J Mater Res Technol* 8: 4066–4078. https://doi.org/10.1016/j.jmrt.2019.07.016
14. Peng L, Stewart MG, Melchers RE (2017) Corrosion and capacity prediction of marine steel infrastructure under a changing environment. *Struct Infrastruct Eng* 13: 988–1001. https://doi.org/10.1080/15732479.2016.1229798
15. Williams PD, Guilyardi E, Madec G, et al. (2010) The role of mean ocean salinity in climate. *Dyn Atmos Oceans* 49: 108–123. https://doi.org/10.1016/j.dynatmoce.2009.02.001

16. Shokri A, Sanavi Fard M (2022) Corrosion in seawater desalination industry: A critical analysis of impacts and mitigation strategies, *Chemosphere* 307: 135640. https://doi.org/10.1016/j.chemosphere.2022.135640
17. Zhang Y, Yan T, Fan L, et al. (2021) Effect of pH on the corrosion and repassivation behavior of TA2 in simulated seawater. *Materials* 14: 6764. https://doi.org/10.3390/ma14226764
18. Gao K, Li D, Pang X, et al. (2010) Corrosion behavior of low-carbon bainitic steel under a constant elastic load. *Corros Sci* 52: 3428–3434. https://doi.org/10.1016/j.corsci.2010.06.021
19. Xu LY, Cheng YF (2012) An experimental investigation of corrosion of X100 pipeline steel under uniaxial elastic stress in a near-neutral pH solution. *Corros Sci* 59: 103–109. https://doi.org/10.1016/j.corsci.2012.02.022
20. Yang S, Yang H, Liu G, et al. (2016) Approach for fatigue damage assessment of welded structure considering coupling effect between stress and corrosion. *Int J Fatigue* 88: 88–95. https://doi.org/10.1016/j.ijfatigue.2016.03.024
21. Xu Y, Huang Y, Cai F, et al. (2020) Study on corrosion behavior and mechanism of AISI 4135 steel in marine environments based on field exposure experiment. *Sci Total Environ* 830: 154864. https://doi.org/10.1016/j.scitotenv.2022.154864
22. Tian H, Cui Z, Ma H, et al. (2022) Corrosion evolution and stress corrosion cracking behavior of a low carbon bainite steel in the marine environments: Effect of the marine zones. *Corros Sci* 206: 110490. https://doi.org/10.1016/j.corsci.2022.110490
23. Qiao C, Shen L, Hao L, et al. (2019) Corrosion kinetics and patina evolution of galvanized steel in a simulated coastal-industrial atmosphere. *J Mater Sci Technol* 35: 2345–2356. https://doi.org/10.1016/j.jmst.2019.05.039
24. Refait P, Grolleau A-M, Jeannin M, et al. (2020) Corrosion of carbon steel in marine environments: Role of the corrosion product layer. *Corros Mater Degrad* 1: 198–218. https://doi.org/10.3390/cmd1010010
25. Lanneluc I, Langumier M, Sabot R, et al. (2015) On the bacterial communities associated with the corrosion product layer during the early stages of marine corrosion of carbon steel. *Int Biodeter Biodegr* 99: 55–65. https://doi.org/10.1016/j.ibiod.2015.01.003
26. Pineau S, Sabot R, Quillet L, et al. (2008) Formation of the Fe(II–III) hydroxy sulfate green rust during marine corrosion of steel associated to molecular detection of dissimilatory sulfite-reductase. *Corros Sci* 50: 1099–1111. https://doi.org/10.1016/j.corsci.2007.11.029
27. Refait P, Jeannin M, Fran çois E, et al. (2019) Galvanic corrosion in marine environments: Effects associated with the inversion of the polarity of Zn/carbon steel couples. *Mater Corros* 70: 950–961. https://doi.org/10.1002/maco.201810568
28. Refait P, Grolleau A-M, Jeannin M, et al. (2016) Localized corrosion of carbon steel in marine media: Galvanic coupling and heterogeneity of the corrosion product layer. *Corros Sci* 111: 583–595. https://doi.org/10.1016/j.corsci.2016.05.043
29. Refait P, Jeannin M, Sabot R, et al. (2013) Electrochemical formation and transformation of corrosion products on carbon steel under cathodic protection in seawater. *Corros Sci* 71: 32–36. https://doi.org/10.1016/j.corsci.2013.01.042
30. Refait P, Nguyen DD, Jeannin M, et al. (2011) Electrochemical formation of green rusts in deaerated seawater-like solutions. *Electrochim Acta* 56: 6481–6488. https://doi.org/10.1016/j.electacta.2011.04.123

31. Yan L, Diao Y, Lang Z, et al. (2020) Corrosion rate prediction and influencing factors evaluation of low-alloy steels in the marine atmosphere using machine learning approach. *Sci Technol Adv Mater* 21: 359–370. https://doi.org/10.1080/14686996.2020.1746196
32. Moshtaghi M, Safyari M, Mori G (2022) Hydrogen absorption rate and hydrogen diffusion in a ferritic steel coated with a micro- or nanostructured ZnNi coating. *Electrochem Commun* 134: 107169. https://doi.org/10.1016/j.elecom.2021.107169
33. Rai PK, Shekhar S, Mondal K (2018) Development of gradient microstructure in mild steel and grain size dependence of its electrochemical response. *Corros Sci* 138: 85–95. https://doi.org/10.1016/j.corsci.2018.04.009
34. Loto CA (2017) Microbiological corrosion: mechanism, control, and impact-a review. *Int J Adv Manuf Technol* 92: 4241–4252. https://doi.org/10.1007/s00170-017-0494-8
35. Moradi M, Song Z, Yang L, et al. (2014) Effect of marine *Pseudoalteromonas* sp. on the microstructure and corrosion behavior of 2205 duplex stainless steel. *Corros Sci* 84: 103–112. https://doi.org/10.1016/j.corsci.2014.03.018
36. Vinoth Jebaraj A, Ajaykumar L, Deepak CR, et al. (2017) Weldability, machinability and surfacing of commercial duplex stainless steel AISI2205 for marine applications—A recent review. *J Adv Res* 8: 183–199. https://doi.org/10.1016/j.jare.2017.01.002
37. Wu J, Zhang D, Wang P, et al. (2016) The influence of *Desulfovibrio* sp. and *Pseudoalteromonas* sp. on the corrosion of Q235 carbon steel in natural seawater. *Corros Sci* 112: 552–562. https://doi.org/10.1016/j.corsci.2016.04.047
38. Xianbo S, Xu D, Yan M, et al. (2017) Study on microbiologically influenced corrosion behavior of novel Cu-bearing pipeline steels. *Acta Metall Sin* 53: 153. https://doi.org/10.11900/0412.1961.2016.00143
39. Yuan S, Liang B, Zhao Y, et al. (2013) Surface chemistry and corrosion behavior of 304 stainless steel in simulated seawater containing inorganic sulfide and sulfate-reducing bacteria. *Corros Sci* 74: 353–366. https://doi.org/10.1016/j.corsci.2013.04.058
40. Zhu J, Li D, Chang W, et al. (2020) In situ marine exposure study on corrosion behaviors of five alloys in coastal waters of western Pacific Ocean. *J Mater Res Technol* 9: 8104–8116. https://doi.org/10.1016/j.jmrt.2020.05.060
41. Altomare A, Cuocci C, Giacovazzo C, et al. (2008) QUALX: a computer program for qualitative analysis using powder diffraction data. *J Appl Cryst* 41: 815–817. https://doi.org/10.1107/S0021889808016956
42. Downs RT, Hall-Wallace M (2003) The American mineralogist crystal structure database. *Am Min* 88: 247–250. https://doi.org/10.5860/choice.41sup-0262
43. Singh R (2007) Corrosion evaluation and monitoring practices, *Training Program on Industrial Corrosion: Evaluation and Mitigation*, Jamshedpur: NML Publication, 48–67.
44. Kvarekvål J, Moloney J (2017) 6-Sour corrosion, In: El-Sherik AM, *Trends in Oil and Gas Corrosion Research and Technologies*, Boston: Woodhead Publishing, 113–147. https://doi.org/10.1016/B978-0-08-101105-8.00006-1
45. Grachev VA, Rozen AE, Perelygin YP, et al. (2020) Multilayer corrosion-resistant material based on iron-carbon alloys. *Heliyon* 6: e04039. https://doi.org/10.1016/j.heliyon.2020.e04039
46. Grachev VA, Rozen AE, Perelygin YP, et al. (2019) Accelerated corrosion tests of a new class of multilayer metallic materials with an internal protector. *Russ Metall* 2019: 247–256. https://doi.org/10.1134/S0036029519030030

47. Smith CB, Mishra RS (2014) Chapter 4-Case study of aluminum 5083-H116 alloy, In: Smith CB, Mishra MS, *Friction Stir Processing for Enhanced Low Temperature Formability*, Butterworth-Heinemann, 19–124. https://doi.org/10.1016/B978-0-12-420113-2.00004-0
48. Lyon S (2012) 1-Overview of corrosion engineering, science, and technology, In: Féron D, *Nuclear Corrosion Science and Engineering*, Woodhead Publishing, 3–30. https://doi.org/10.1533/9780857095343.1.3
49. Chen S, Zhang D (2019) Corrosion behavior of Q235 carbon steel in air-saturated seawater containing *Thalassospira* sp. *Corros Sci* 148: 71–82. https://doi.org/10.1016/j.corsci.2018.11.031
50. Fardilah VA, Pusparizkita YM, Aslan C, et al. (2022) Assessment on the pitting-corrosion of 1037-mild carbon steel by bacteria in B30 biodiesel product. *J Bio- Tribo-Corros* 8: 92. https://doi.org/10.1007/s40735-022-00693-x
51. Cui Z, Chen S, Dou Y, et al. (2019) Passivation behavior and surface chemistry of 2507 super duplex stainless steel in artificial seawater: Influence of dissolved oxygen and pH. *Corros Sci* 150: 218–234. https://doi.org/10.1016/j.corsci.2019.02.002
52. Herrera LK, Videla HA (2009) Role of iron-reducing bacteria in corrosion and protection of carbon steel. *Int Biodeterior Biodegrad* 63: 891–895 https://doi.org/10.1016/j.ibiod.2009.06.003
53. Dubiel M, Hsu CH, Chien CC, et al. (2002) Microbial iron respiration can protect steel from corrosion. *Appl Environ Microbiol* 68: 1440–1445. https://doi.org/10.1128/AEM.68.3.1440-1445.2002
54. Wang X, Melchers RE (2017) Corrosion of carbon steel in presence of mixed deposits under stagnant seawater conditions. *J Loss Prev Process Ind* 45: 29–42. https://doi.org/10.1016/j.jlp.2016.11.013
55. Fuente de la D, Alcántara J, Chico B, et al. (2016) Characterization of rust surfaces formed on mild steel exposed to marine atmospheres using XRD and SEM/Micro-Raman techniques. *Corros Sci* 110: 253–264. https://doi.org/10.1016/j.corsci.2016.04.034
56. Su Y, Shi Y, Li Y, et al. (2023) Corrosion behavior on carbon steel affected by iron-reducing bacteria via dissimilatory Fe(III) reduction in simulated marine atmospheric environment. *Corros Sci* 220: 111283. https://doi.org/10.1016/j.corsci.2023.111283
57. Dec W, Mosiałek M, Socha RP, et al. (2017) Characterization of desulfovibrio desulfuricans biofilm on high-alloyed stainless steel: XPS and electrochemical studies. *Mater Chem Phys* 195: 28–39. https://doi.org/10.1016/j.matchemphys.2017.04.011
58. Mohammadikish M (2014) Hydrothermal synthesis, characterization and optical properties of ellipsoid shape α-Fe_2O_3 nanocrystals. *Ceram Int* 40: 1351–1358. https://doi.org/10.1016/j.ceramint.2013.07.016
59. Antunes RA, Costa I, de Faria DLA (2003) Characterization of corrosion products formed on steels in the first months of atmospheric exposure. *Mat Res* 8: 403–406. https://doi.org/10.1590/S1516-14392003000300015
60. Tian F, He X, Bai X, et al. (2020) Electrochemical corrosion behaviors and mechanism of carbon steel in the presence of acid-producing bacterium *Citrobacter farmeri* in artificial seawater. *Int Biodeterior Biodegrad* 147: 104872. https://doi.org/10.1016/j.ibiod.2019.104872
61. Liu H, Chen C, Asif M, et al. (2022) Mechanistic investigations of corrosion and localized corrosion of X80 steel in seawater comprising sulfate-reducing bacteria under continuous carbon starvation. *Corros Commun* 8: 70–80. https://doi.org/10.1016/j.corcom.2022.08.002

62. Sherif ESM, Erasmus RM, Comins JD (2010) In situ Raman spectroscopy and electrochemical techniques for studying corrosion and corrosion inhibition of iron in sodium chloride solutions. *Electrochim Acta* 55: 3657–3663. https://doi.org/10.1016/j.electacta.2010.01.117
63. Oh SJ, Cook DC, Townsend HE (1998) Characterization of iron oxides commonly formed as corrosion products on steel. *Hyperfine Interact* 112: 59–66. https://doi.org/10.1023/A:1011076308501
64. Sherif ESM (2014) A Comparative study on the electrochemical corrosion behavior of iron and X-65 steel in 4.0 wt% sodium chloride solution after different exposure intervals. *Molecules* 19: 9962–9974. https://doi.org/10.3390/molecules19079962
65. Alcántara J, de la Fuente D, Chico B, et al. (2017) Marine atmospheric corrosion of carbon steel: A review. *Materials* 10: 406. https://doi.org/10.3390/ma10040406
66. Gehring AU, Hofmeister AM (1994) The transformation of lepidocrocite during heating: A magnetic and spectroscopic study. *Clays Clay Miner* 42: 409–415. https://doi.org/10.1346/CCMN.1994.0420405
67. Dwivedi D, Lepkova K, Becker T (2017) Carbon steel corrosion: a review of key surface properties and characterization methods. *RSC Adv* 7: 4580–4610. https://doi.org/10.1039/c6ra25094g
68. Cui Z, Chen S, Wang L, et al. (2017) Passivation behavior and surface chemistry of 2507 super duplex stainless steel in acidified artificial seawater containing thiosulfate. *J Electrochem Soc* 164: C856. https://doi.org/10.1149/2.1901713jes

AIMS Press